Nuclear Instruments and Methods in Physics Research A 830 (2016) 375–380

Contents lists available at ScienceDirect

Nuclear Instruments and Methods in Physics Research A

journal homepage: www.elsevier.com/locate/nima

Control and optimization of a staged laser-wakefield accelerator

G. Golovin, S. Banerjee, S. Chen, N. Powers [1], C. Liu, W. Yan, J. Zhang, P. Zhang, B. Zhao, D. Umstadter *

Physics and Astronomy Department, University of Nebraska-Lincoln, Lincoln, NE 68508, USA

ARTICLE INFO

Article history:
Received 3 May 2016
Accepted 6 June 2016
Available online 7 June 2016

Keywords:
Laser wakefield acceleration
Ionization-assisted injection

ABSTRACT

We report results of an experimental study of laser-wakefield acceleration of electrons, using a staged device based on a double-jet gas target that enables independent injection and acceleration stages. This novel scheme is shown to produce stable, quasi-monoenergetic, and tunable electron beams. We show that optimal accelerator performance is achieved by systematic variation of five critical parameters. For the injection stage, we show that the amount of trapped charge is controlled by the gas density, composition, and laser power. For the acceleration stage, the gas density and the length of the jet are found to determine the final electron energy. This independent control over both the injection and acceleration processes enabled independent control over the charge and energy of the accelerated electron beam while preserving the quasi-monoenergetic character of the beam. We show that the charge and energy can be varied in the ranges of 2–45 pC, and 50–450 MeV, respectively. This robust and versatile electron accelerator will find application in the generation of high-brightness and controllable x-rays, and as the injector stage for more conventional devices.

1. Introduction

Laser wakefield acceleration (LWFA) has been developing dramatically over the past decades, from a conceptual notion [1] into a rapidly maturing field [2–4]. The motivation for using LWFA electron sources is that the acceleration gradient is two to three orders of magnitude higher than conventional radio frequency linear accelerators; therefore, high-energy electrons can be accelerated with a much smaller footprint. Other useful characteristics of laser-accelerated electrons include extremely short fs-level duration [5], and ultra-small bunch emittance [6,7].

Numerous applications require stable, energetic *e*-beams exhibiting high charge, low energy spread, and broad energy tunability. Those characteristics have been difficult to achieve simultaneously in single-stage LWFA with self-trapping because of the differing requirements for the injection and acceleration processes. For example, acceleration of high energy electrons requires a low-density plasma because of its longer dephasing length ($L_{\mathrm{deph}} \propto n^{-3/2}$, where n is the plasma density) and depletion length ($L_{\mathrm{depl}} \propto n^{-1}$) [8]. At the same time, self-trapping in a low-density plasma is ineffective in terms of injected charge and provides little control over generated electron beams. To overcome this issue, various approaches have been introduced, in order to achieve controlled injection [9]. These methods do not rely on self-trapping, but instead involve deterministically forcing background plasma electrons to become locally dephased with respect to the wakefield and thus get trapped, and eventually accelerated by, the plasma wave. One implementation of this general concept involves the use of additional laser pulses [10–13]; while another involves the use of a density ramp [14–20]. Although the injector and accelerator stages were physically separated in some of these experiments [21–27], in the majority of cases, the injection and acceleration processes were not independently controlled, and consequently, neither were the electron beam parameters.

We have recently proposed an alternative design of a staged LWFA target, consisting of two overlapped gas jets: the “injector”, operated with mixed gas (helium with a small percentage of nitrogen); and the “accelerator”, operated with pure helium [28]. The two jets form a plasma density profile with three regions (see Fig. 1). Region I is a density up-ramp, comprised of mixed gas. While propagating through this region, a laser pulse experiences self-focusing and self-steepening, forming a bubble in the plasma. Since on a density up-ramp the bubble shrinks, the injection process is prohibited [29]. Region II is a density down-ramp, also comprised of mixed gas. In this region, ionization-assisted injection, as well as density-down-ramp and self-injection, is possible. Region III is a density down-ramp, composed of pure helium. In this region, ionization-assisted injection cannot happen (since

* Correspondence to: 501 Building, Rm 38, Lincoln, NE 68588-0207, USA.
E-mail address: donald.umstadter@unl.edu (D. Umstadter).
[1] Present address: Physics and Astronomy Department, Brigham Young University, Provo, UT 84602, USA.

http://dx.doi.org/10.1016/j.nima.2016.06.022

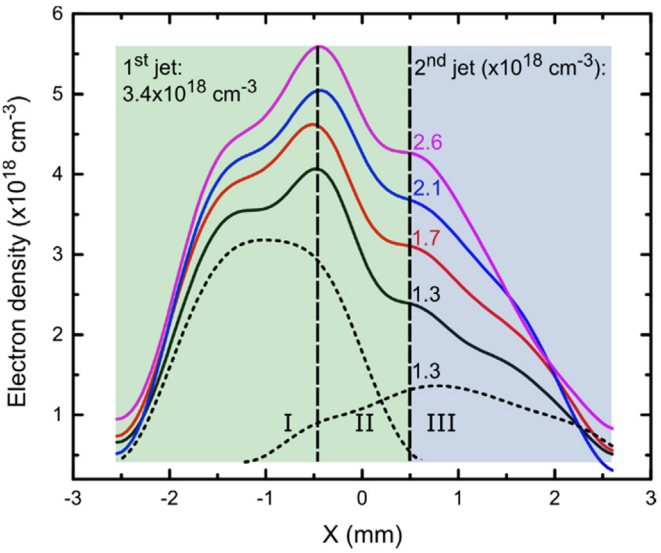

Fig. 1. Density profiles of the double-jet gas target. The 1st jet (0.5-mm-long nozzle) density is fixed ($n_{1e}=3.4\times10^{18}$ cm^{-3}), the 2nd jet (2-mm-long nozzle) density is varied ($n_{2e}=1.3$–2.6×10^{18} cm^{-3}). Dotted lines show the 1st (at the left) and the 2nd (at the right) individual jet density profiles. The dashed lines separate the double-jet profile into three regions. Region I: up-ramp (mixed gas); region II: down-ramp (mixed gas); region III: down-ramp (pure helium). Green shaded area (regions I and II) corresponds to the area where nitrogen is presented. Blue shaded area (region III) corresponds to the area with pure helium. (For interpretation of the references to color in this figure legend, the reader is referred to the web version of this article.)

there are no nitrogen atoms), but self-injection or down-ramp injection might occur; previously injected electrons are also accelerated in this region. The idea of the double-jet target design is to restrict injection in the short region II and acceleration in the long region III, which allows for independent control over both processes. As we have experimentally shown [28,30], this design indeed leads to generation of stable, quasi-monoenergetic *e*-beams with a very high degree of control (Fig. 1).

In this paper, we examine the significant capabilities of this novel design. We show that there are five essential parameters associated with the staged acceleration device that can be used to precisely determine the electron beam characteristics. Three parameters (injector jet density, atomic composition, and laser pulse power) control the amount of trapped charge, while two other parameters (accelerator jet density and length) control its subsequent acceleration (acceleration gradient and length, respectively). Each of these parameters are independently controllable and highly reproducible leading to clear demonstration of a system that can be tuned and optimized in a straightforward way. We have studied in detail the dependence of the electron beam characteristics on each of these parameters and have quantified the extent of control that is thereby provided in our acceleration system.

2. Experimental setup

For the experiments reported here, we used the Diocles laser system (805 nm central wavelength, 10 Hz repetition rate) that delivered 34 fs pulses with up to 1.7 J of laser energy per pulse on target, which corresponds to a peak power of 50 TW [31]. A closed-loop technique for temporal phase correction [32] was used to achieve a Fourier-limited pulse duration. Laser pulses were focused by an f/14 off-axis parabola (1 m focal length) to a 20-um diameter focal spot (FWHM) with 30% of the energy contained within the FWHM contour. A deformable mirror compensated the

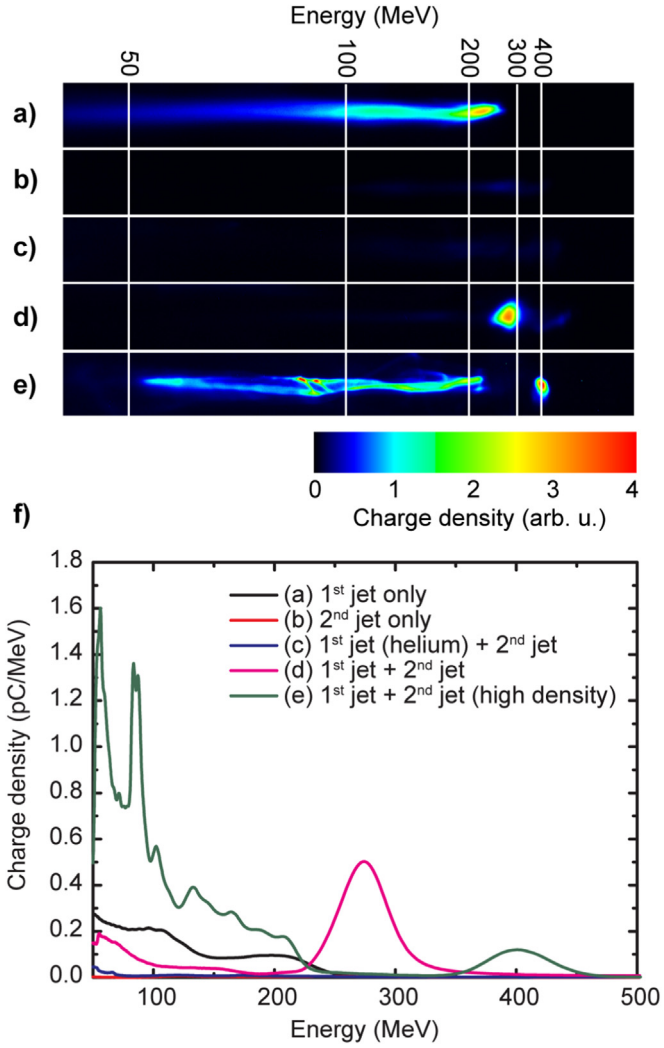

Fig. 2. Lanex images (a–e) and corresponding electron beam spectra (f) for different working regimes of the double-jet. The nozzles are 0.5 and 2 mm long. The 1st jet utilizes 1% mixed gas (if not specified), the 2nd jet – pure helium. a) 1st jet only, $n_{1e}=3.4\times10^{18}$ cm^{-3}; b) 2nd jet only, $n_{2e}=1.7\times10^{18}$ cm^{-3}; c) both jets operated with helium, $n_{1e}=3.4\times10^{18}$ cm^{-3}, $n_{2e}=1.7\times10^{18}$ cm^{-3}; d) the same as (c), but the 1st jet operated with 1% mixed gas; e) 1st jet operated with 1% mixed gas, $n_{1e}=3.4\times10^{18}$ cm^{-3}, 2nd jet operated with helium, $n_{2e}=2.6\times10^{18}$ cm^{-3}.

optical aberrations of the laser wavefront and a near diffraction limited spot is obtained [33].

The target consisted of two slit nozzles separated by 0.5 mm gap. The first jet (injector, 0.5-mm-long nozzle) utilized He/N_2 gas mixture with 99/1 or 95/5 relative densities. The second one (accelerator, 0.5, 2, or 4-mm-long nozzles) utilized pure helium. While using the 2-mm-long accelerator nozzle, we covered its exit side with a razor blade. By tuning the blade position, we controlled the length of the accelerator stage. Laser pulses were focused on the rising edge of the injector jet at a height of 2 mm above the nozzle orifices. Neutral gas 3D density profiles of both individual jets and the double-jets were measured by a Mach–Zehnder interferometer and reconstructed using the SIRT tomography method [34]. Some profiles relevant to the work presented in this paper are shown in Fig. 1. A magnetic spectrometer (a 7.5 in. 0.8 T magnet and a Lanex screen, imaged by a 12 bit camera), was used to analyze *e*-beam spectra. To characterize higher energy (200–400 MeV) *e*-beams, we added a second magnet (6 in. 0.7 T). The magnetic spectrometer had an energy resolution of 2% at 60 MeV, and 4% at 400 MeV.

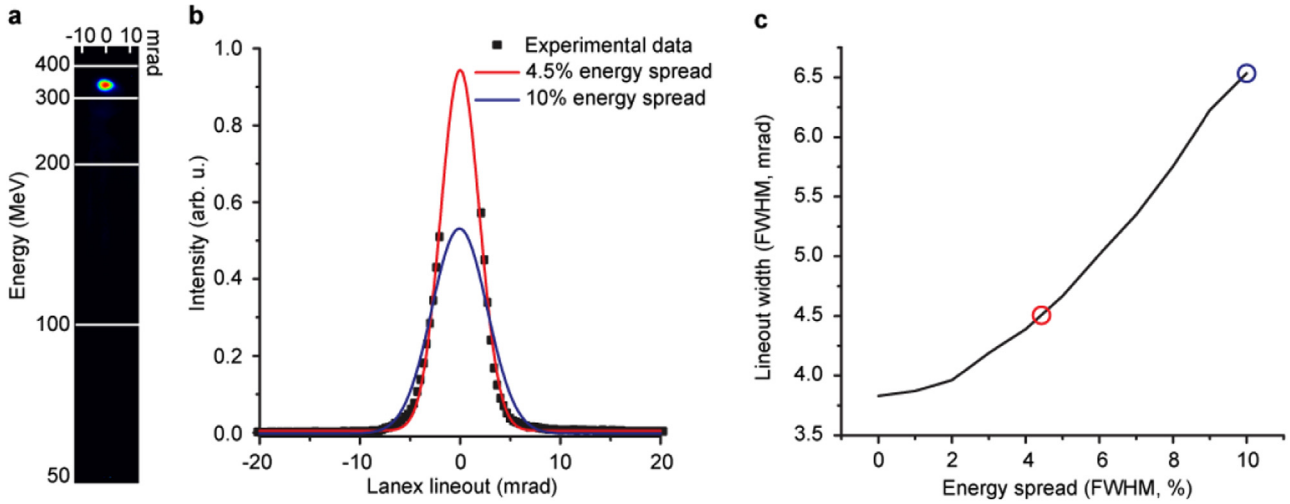

Fig. 3. Electron beam energy spread and divergence deconvolution. a) Dispersed Lanex image of a single shot. Central energy – 320 MeV, divergence – 4.6 mrad. 1st jet operated with 1% mixed gas ($n_{1e}=3.4\times10^{18}$ cm^{-3}), 2nd – with pure helium ($n_{2e}=2.3\times10^{18}$ cm^{-3}). b) Lanex lineout along the dispersion axis. "0 mrad" corresponds to central energy (320 MeV). Two solid lines show simulations with different electron beam energy spreads. c) Simulated lineout width as a function of electron beam energy spread. Two colored circles mark two widths shown on (b). (For interpretation of the references to color in this figure legend, the reader is referred to the web version of this article.)

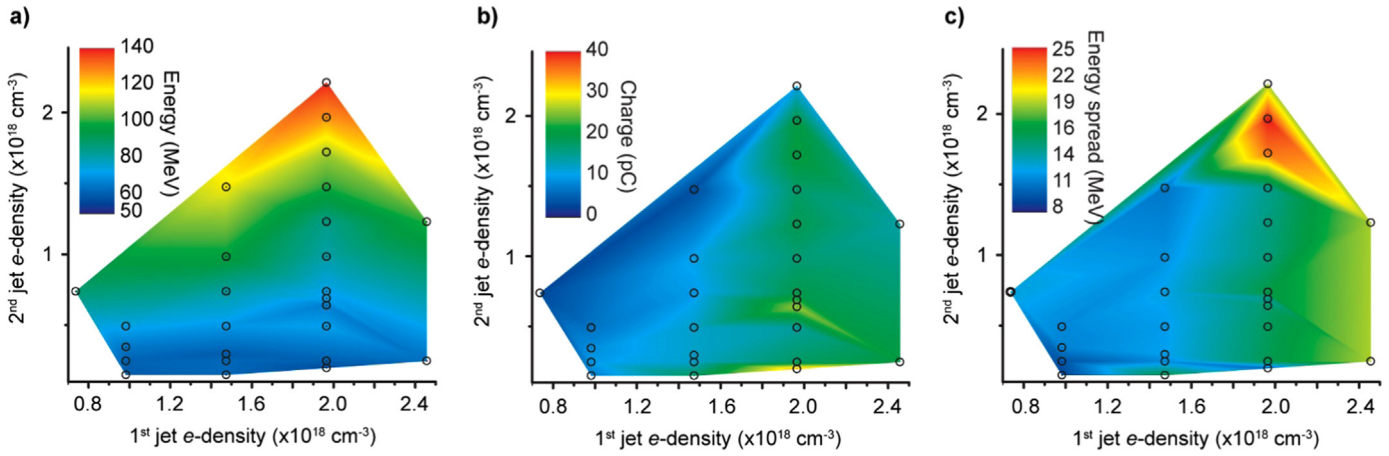

Fig. 4. Central energy (a) charge (b) and energy spread (c) of the generated electron beams as a function of the 1st and 2nd jet densities. 1st jet operated with 1% mixed gas, 2nd jet (0.5 mm long) with pure helium.

3. Quasi-monoenergetic beams from staged accelerator

The staging concept permits operation of our device with a range of parameters that permits access to different regimes of acceleration. In the simplest possible case, we fired the first (injector) jet only (with mixed gas), keeping the accelerator jet turned off and we observed electron beams with continuous spectra, as shown in Fig. 2a. The broadband energy spectrum is due to continuous ionization-assisted injection. The second (accelerator) jet, fired with pure helium alone, did not produce any significant amount of charge (see Fig. 2b) because it was operated such that the plasma density is below the threshold for self-injection. When both jets were fired with pure helium, we again did not observe any accelerated charge (see Fig. 2c), which means that no down-ramp or self-injection occurred. The situation changed dramatically when we fired the first jet with mixed gas, and the second with pure helium (see Fig. 2d), which resulted in generation of quasi-monoenergetic electron bunches.

When we further increased the density of the accelerator jet, we observed electron beams with two features in the spectra: quasi-monoenergetic component, and polychromatic tail (see Fig. 2e). This polychromatic tail appeared when the 2nd jet density was more than 2.6×10^{18} cm^{-3} (at 3.4×10^{18} cm^{-3} for the 1st jet density). For overall density profile, it corresponds to $\sim5.5\times10^{18}$ cm^{-3} threshold value (see Fig. 1, purple curve). The polychromatic feature can be attributed to self-injection in region III of the double-jet, which happened in addition to ionization-assisted injection in region II. According to Mangles et al. [35], self-injection happens when

$$\alpha E > \frac{\pi\varepsilon_0 m_e^2 c^5}{q_e^2}\left[\log\left(\frac{2n_c}{3n}\right)-1\right]^3\frac{n_c}{n}\tau(l),$$

where α is the fraction of laser energy E within FWHM of focal spot, ε_0 is free space permittivity, q_e and m_e are electron charge and mass, n_c is plasma critical density, and n is plasma density. Laser pulse duration $\tau(l)$ after propagation of distance l can be estimated as $\tau(l)=\tau_0 - nl/2cn_c$, where τ_0 is initial pulse duration [36]. For $\alpha=0.3$, $E=1.7$ J, and $l=3$ mm this estimate gives 6×10^{18} cm^{-3} electron density as a threshold, which matches the experimentally measured value.

Electron beams with narrow energy spreads require careful processing, since energy spread and beam divergence are convolved on

the detector after dispersion in the magnetic spectrometer. Deconvolution was necessary when angular sizes of an electron beam along the dispersion axis and perpendicular to it were comparable. Fig. 3 illustrates the way it was accomplished. We started with a dispersed Lanex image (Fig. 3a) and calculated angular size of the e-beam perpendicular to the dispersion axis (divergence). We plotted the beam intensity profile along the dispersion axis (Fig. 3b, points). We then simulated propagation of an electron beam through the magnetic spectrometer for constant divergence and different energy widths (Fig. 3c) and found energy spread, which resulted in optimal fit of the experimentally measured intensity profile. For the particular shot shown in Fig. 3, straightforward energy spread determination (without deconvolution) yielded 10% (FWHM), while deconvolution was 5% (upper limit).

4. Multi-parameter control of electron beam characteristics

In this section, we discuss the five parameters that can be varied for our device and show their role in the control of electron beam characteristics.

The first two parameters are the densities of the 1st and 2nd gas jets. Electron beam central energy, charge, and energy spread are shown in Fig. 4 as a function of these parameters. As one can see in Fig. 4a, central energy of the generated electron beams depends on the 2nd jet density, and does not depend on the 1st jet density. It shows that the acceleration process happens primarily in region III of the double-jet density profile, which is controlled by the 2nd jet only. Central energy of the electron beams grows with the density of this region since the accelerating field (E_{acc}) grows with plasma density [37]: $E_{acc} \propto \sqrt{n_e}$. It also indicates that the acceleration length does not reach dephasing length, otherwise we would observe the opposite dependence: $E_{max} \propto n_e^{-2/3}$, where E_{max} is the maximal energy reached by the electron bunch, accelerated over full dephasing length [8].

At the same time, electron beam charge depends on the 1st jet density, and does not depend on the 2nd jet density (see Fig. 4b). Since trapping happens in region II and is due to ionization-assisted injection process [28], this dependence can be explained simply by the fact that trapped charge depends on the amount of nitrogen in this region. Indeed, the amount of nitrogen depends linearly on the 1st jet density (operated with mixed gas), and does not depend on the 2nd jet density (operated with helium). It is important to note that even though region II is actually an overlap of the 1st and 2nd jets (see Fig. 1), it is only the 1st jet which controls the amount of injected charge, since nitrogen is presented only in that jet.

Energy spread of the electron beams depends on both 1st and 2nd jet densities (see Fig. 4c); its behavior is a complicated interplay of multiple effects. First, the length of the region II (injection region) slightly depends on both jet densities, and the energy spread is proportional to this length. Second, accelerating field in that region $E_{acc} \propto \sqrt{n_e}$ depends on total density, which is again a function of both jet densities. Third, final energy spread is strongly affected by subsequent acceleration in region III (so called "phase-space rotation"), so it is sensitive to the 2nd jet density.

The third parameter of the double-jet design is the 2nd jet length, which defines the length of region III, where the main acceleration happens. For the 2nd, we used 0.5, 2, and 4 mm nozzles to study the role of this parameter. In addition, we put a razor blade on the rear end of the 2 mm nozzle, and controlled its length by tuning the blade position (1 and 1.5 mm). The results are shown in Fig. 5. At a given density of the 2nd jet, which defines the acceleration gradient, central energy of the accelerated electron beam scales with the length of the 2nd gas jet, since this length controls how long an electron bunch is exposed to the acceleration gradient.

The fourth parameter of the double-jet target design is the nitrogen percentage in the 1st jet. Since trapping happens via ionization-assisted injection mechanism, one should expect an increase of injected charge when nitrogen concentration goes up. To prove that, we performed the following experiment. We fixed the 1st jet density at $n_{1e}=3.4\times10^{18}$ cm^{-3}, and 2nd jet density at

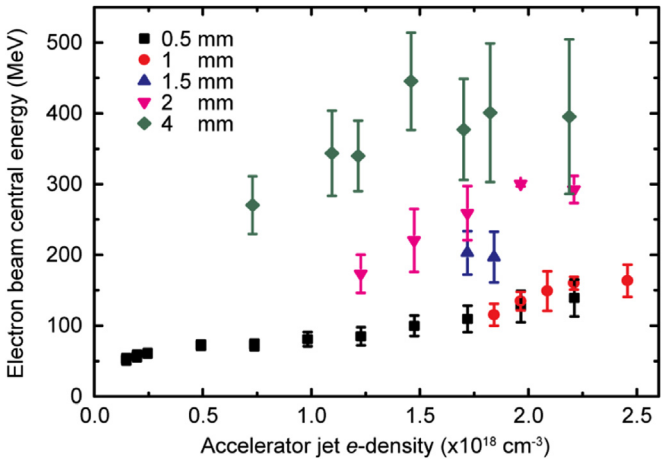

Fig. 5. Central energy of the electron beams, accelerated with different lengths of the 2nd jet. The 1st jet utilizes 1% mixed gas ($n_{1e}=2.0\times10^{18}$ cm^{-3} for 0.5 mm 2nd nozzle, $n_{1e}=3.4\times10^{18}$ cm^{-3} for 1–4 mm 2nd nozzles), the 2nd jet uses pure helium. The error bars here and on the subsequent figures represent standard deviation calculated from sets of shots.

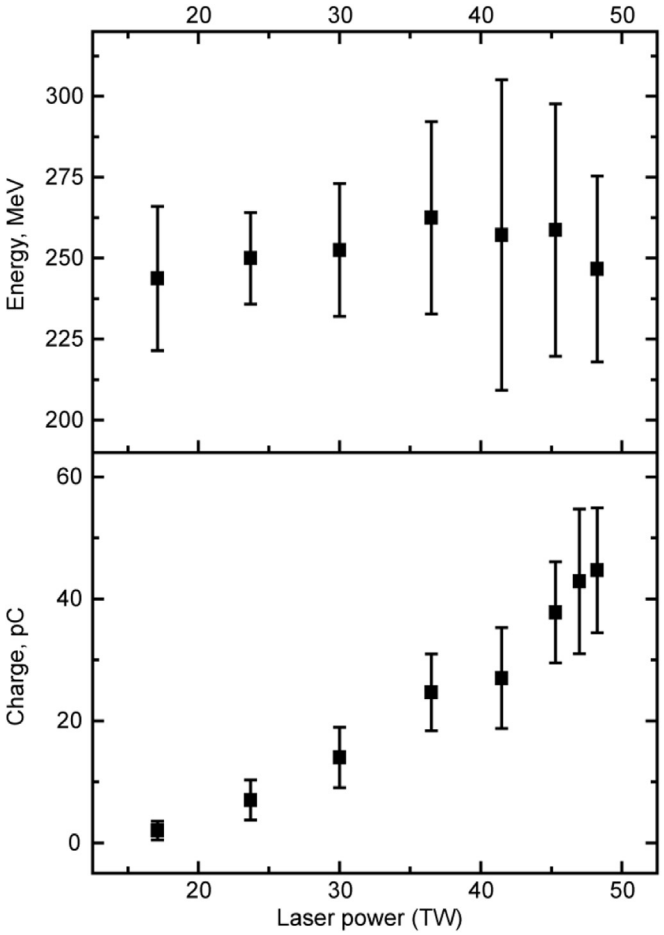

Fig. 6. Electron beams charge tuning with laser power. 1st jet (5% mixed gas) density $n_{1e}=3.4\times10^{18}$ cm^{-3}, 2nd jet (2 mm long) density $n_{2e}=2.4\times10^{18}$ cm^{-3}.

Table 1
Overview of the experimental results.

Double-jet parameters					*Electron-beam properties*		
Injector jet density, cm^{-3}	*Injector jet nitrogen concentration, %*	*Accelerator jet density, cm^{-3}*	*Accelerator jet length, mm*	*Laser power, TW*	*Central energy, MeV*	*Energy spread (FWHM), %*	*Charge, pC*
1.0-2.5 x 10^{18}	1	1.0 x 10^{18}	0.5	48	62-64	16-31	9-20
3.4 x 10^{18}	1-5	2.4 x 10^{18}	2	48	290-250		16-44
2.0 x 10^{18}	1	0.2-2.0 x 10^{18}	0.5	48	61-127	16-16	18-20
2.0-3.4 x 10^{18}	1	1.5 x 10^{18}	0.5-4	48	100-445	14-22	17-16
3.4 x 10^{18}	5	2.4 x 10^{18}	2	17-48	244-247	9-12	2-45

$n_{2e}=2.4\times10^{18}$ cm^{-3} (2 mm long nozzle). When the 1st jet was operated with 1% mixed gas (so helium-to-nitrogen ratio was 99-to-1), we observed electron beams with averaged charge of 16 ± 6 pC and central energy of 290 ± 20 MeV. When it was operated with 5% mixed gas, the charge went up to 44 ± 10 pC, and central energy slightly decreased to 250 ± 30 MeV. The increase of nitrogen concentration by a factor of 5 led to the increase of charge by a factor of 3, and to the decrease in central energy by 14%. This deviation from linear behavior (when charge is proportional to the nitrogen concentration) and slight decrease in final energy might by explained with the effect of beam loading [38], when the electric field of a trapped electron bunch modifies the field of the bubble, affecting further injection and decreasing accelerating gradient.

The last parameter of our experiment is laser power, even though it belongs to the laser system and not to the double-jet gas target. Central energy and charge of the accelerated electron beams as a function of laser power is shown in Fig. 6. As one can see, central energy stays constant while we change laser power, and charge depends on it linearly. The first is due to the fact that accelerating gradient does not depend on laser power. The second can be explained in the following way. The amount of trapped charge in ionization-assisted injection depends on the volume of the laser pulse, where its intensity reaches the threshold of over-the-barrier ionization. Since this volume grows with laser power, trapped charge should also grow with it, as we see in the experiment. It is interesting to note that ionization-assisted injection in nitrogen requires a minimum normalized laser field of a_0~1.7 (for ionization of N^{6+} electrons) [37]. Without self-focusing, it corresponds to 47 TW of laser power (with our laser beam size and focusing optics). Since we observed ionization-assisted injection starting at only 17 TW, it is a clear indication of self-focusing in our experiments even at lowest values of laser power. This is not surprising, given that self-focusing critical power for plasma density of 3×10^{18} cm^{-3} (an average density of the double-jet for Fig. 6) is 10 TW.

All five parameters of the double-jet gas target, as well as their effect on the electron beams, are summarized in Table 1. Every row corresponds to an experimental scan, where a single parameter of the double-jet is varied, while all the rest are kept fixed (an exception is made for the accelerator jet length scan, when different densities of the injector jet were used for the 0.5 and 4-mm-long accelerator jets). The cells with parameters being varied are highlighted in blue. Three columns at the right represent the ranges of the generated electron beams properties, with the first number corresponding to the lowest value of the double-jet parameter, and the second number to the highest one. The properties affected the most are highlighted in orange. The table contains the data shown and discussed before, but gives an overview of the tunability and controllability of the generated electron beams in a concise way.

5. Conclusions

In this work, we explored the control over electron beams enabled by a staged acceleration device based on double-jet gas targets. We identified five parameters of the double-jet target design and studied how each affects the parameters of the generated electron beams. We found that the electron beam's central energy can be controlled by means of variation of the 2nd jet plasma density and length, and its charge, by the 1st jet plasma density and nitrogen concentration, as well as by variation of the laser power. Our experiment shows that, with the double-jet target design, electron beam energy and charge can be independently controlled, as a result of independent control over the injection and acceleration processes.

Acknowledgements

This material is based on work supported by the US Department of Energy (DOE), Office of Science, Basic Energy Sciences (BES), under Award #DE-FG02-05ER15663 (ultrafast x-ray science); the Air Force Office for Scientific Research, FA9550-11-1-0157 (high-field laser-electron scattering); the Department of Homeland Security Domestic Nuclear Detection Office, under competitively awarded contract HSHQDC-13-C-B0036 (low-dose x-ray radiography); and the National Science Foundation under Grant no. PHY-153700 (ultra-low emittance electron beams). This support does not constitute an express or implied endorsement on the part of the Government.

References

[1] T. Tajima, J. Dawson, Laser electron accelerator, Phys. Rev. Lett. 43 (1979) 267–270, http://dx.doi.org/10.1103/PhysRevLett.43.267.
[2] E. Esarey, C. Schroeder, W. Leemans, Physics of laser-driven plasma-based electron accelerators, Rev. Mod. Phys. 81 (2009) 1229–1285, http://dx.doi.org/10.1103/RevModPhys.81.1229.
[3] K. Krushelnick, V. Malka, Laser wakefield plasma accelerators, Laser Photon. Rev. 4 (2010) 42–52, http://dx.doi.org/10.1002/lpor.200810062.
[4] V. Malka, Laser plasma accelerators, Phys. Plasmas 19 (2012) 055501, http://dx.doi.org/10.1063/1.3695389.
[5] O. Lundh, J. Lim, C. Rechatin, L. Ammoura, A. Ben-Ismaïl, X. Davoine, G. Gallot, J.-P. Goddet, E. Lefebvre, V. Malka, J. Faure, Few femtosecond, few kiloampere electron bunch produced by a laser–plasma accelerator, Nat. Phys. 7 (2011) 0219–0222, http://dx.doi.org/10.1038/nphys1872.
[6] G. Golovin, S. Banerjee, C. Liu, S. Chen, J. Zhang, B. Zhao, P. Zhang, M. Veale, M. Wilson, P. Seller, D. Umstadter, Intrinsic beam emittance of laser-accelerated electrons measured by x-ray spectroscopic imaging, Sci. Rep. 6 (2016) 24622, http://dx.doi.org/10.1038/srep24622.
[7] R. Weingartner, S. Raith, A. Popp, S. Chou, J. Wenz, K. Khrennikov, M. Heigoldt, A.R. Maier, N. Kajumba, M. Fuchs, B. Zeitler, F. Krausz, S. Karsch, F. Grüner, Ultralow emittance electron beams from a laser-wakefield accelerator, Phys. Rev. Spec. Top. – Accel. Beams 15 (2012) 111302, http://dx.doi.org/10.1103/PhysRevSTAB.15.111302.
[8] W. Lu, M. Tzoufras, C. Joshi, F. Tsung, W. Mori, J. Vieira, R. Fonseca, L. Silva, Generating multi-GeV electron bunches using single stage laser wakefield acceleration in a 3D nonlinear regime, Phys. Rev. Spec. Top. – Accel. Beams 10 (2007) 061301, http://dx.doi.org/10.1103/PhysRevSTAB.10.061301.

[9] D. Umstadter, J. Kim, E. Dodd, Laser injection of ultrashort electron pulses into wakefield plasma waves, Phys. Rev. Lett. 76 (1996) 2073–2076, http://dx.doi.org/10.1103/PhysRevLett.76.2073.
[10] J. Faure, C. Rechatin, A. Norlin, A. Lifschitz, Y. Glinec, V. Malka, Controlled injection and acceleration of electrons in plasma wakefields by colliding laser pulses, Nature 444 (2006) 737–739, http://dx.doi.org/10.1038/nature05393.
[11] C. Rechatin, J. Faure, A. Ben-Ismail, J. Lim, R. Fitour, A. Specka, H. Videau, A. Tafzi, F. Burgy, V. Malka, Controlling the phase-space volume of injected electrons in a laser-plasma accelerator, Phys. Rev. Lett. 102 (2009) 1–4, http://dx.doi.org/10.1103/PhysRevLett.102.164801.
[12] S. Fourmaux, S. Corde, K. Ta Phuoc, P.M. Leguay, S. Payeur, P. Lassonde, S. Gnedyuk, G. Lebrun, C. Fourment, V. Malka, S. Sebban, A. Rousse, J.C. Kieffer, Demonstration of the synchrotron-type spectrum of laser-produced Betatron radiation, New J. Phys. 13 (2011) 033017, http://dx.doi.org/10.1088/1367-2630/13/3/033017.
[13] M. Hansson, B. Aurand, H. Ekerfelt, A. Persson, O. Lundh, Injection of electrons by colliding laser pulses in a laser wakefield accelerator, Nucl. Instrum. Methods Phys. Res. Sect. A Accel. Spectrom. Detect. Assoc. Equip. (2016), http://dx.doi.org/10.1016/j.nima.2016.02.070.
[14] P. Brijesh, C. Thaury, K.T. Phuoc, S. Corde, G. Lambert, V. Malka, S.P.D. Mangles, M. Bloom, S. Kneip, Tuning the electron energy by controlling the density perturbation position in laser plasma accelerators, Phys. Plasmas 19 (2012) 063104, http://dx.doi.org/10.1063/1.4725421.
[15] S. Fourmaux, K. Ta Phuoc, P. Lassonde, S. Corde, G. Lebrun, V. Malka, A. Rousse, J.C. Kieffer, Quasi-monoenergetic electron beams production in a sharp density transition, Appl. Phys. Lett. 101 (2012) 111106, http://dx.doi.org/10.1063/1.4752114.
[16] J. Faure, C. Rechatin, O. Lundh, L. Ammoura, V. Malka, Injection and acceleration of quasimonoenergetic relativistic electron beams using density gradients at the edges of a plasma channel, Phys. Plasmas 17 (2010) 083107, http://dx.doi.org/10.1063/1.3469581.
[17] M. Burza, A. Gonoskov, K. Svensson, F. Wojda, A. Persson, M. Hansson, G. Genoud, M. Marklund, C.-G. Wahlström, O. Lundh, Laser wakefield acceleration using wire produced double density ramps, Phys. Rev. Spec. Top. – Accel. Beams 16 (2013) 011301, http://dx.doi.org/10.1103/PhysRevSTAB.16.011301.
[18] K. Schmid, A. Buck, C. Sears, J. Mikhailova, R. Tautz, D. Herrmann, M. Geissler, F. Krausz, L. Veisz, Density-transition based electron injector for laser driven wakefield accelerators, Phys. Rev. Spec. Top. – Accel. Beams 13 (2010) 1–5, http://dx.doi.org/10.1103/PhysRevSTAB.13.091301.
[19] A. Buck, J. Wenz, J. Xu, K. Khrennikov, K. Schmid, M. Heigoldt, J.M. Mikhailova, M. Geissler, B. Shen, F. Krausz, S. Karsch, L. Veisz, Shock-front injector for high-quality laser-plasma acceleration, Phys. Rev. Lett. 110 (2013) 185006, http://dx.doi.org/10.1103/PhysRevLett.110.185006.
[20] M. Hansson, B. Aurand, X. Davoine, H. Ekerfelt, K. Svensson, A. Persson, C.-G. Wahlström, O. Lundh, Down-ramp injection and independently controlled acceleration of electrons in a tailored laser wakefield accelerator, Phys. Rev. Spec. Top. – Accel. Beams 18 (2015) 071303, http://dx.doi.org/10.1103/PhysRevSTAB.18.071303.
[21] A.J. Gonsalves, K. Nakamura, C. Lin, D. Panasenko, S. Shiraishi, T. Sokollik, C. Benedetti, C.B. Schroeder, C.G.R. Geddes, J. van Tilborg, J. Osterhoff, E. Esarey, C. Toth, W.P. Leemans, Tunable laser plasma accelerator based on longitudinal density tailoring, Nat. Phys. 7 (2011) 862–866, http://dx.doi.org/10.1038/nphys2071.
[22] J. Liu, C. Xia, W. Wang, H. Lu, C. Wang, A. Deng, W. Li, H. Zhang, X. Liang, Y. Leng, X. Lu, C. Wang, J. Wang, K. Nakajima, R. Li, Z. Xu, All-optical cascaded laser wakefield accelerator using ionization-induced injection, Phys. Rev. Lett. (2011), http://dx.doi.org/10.1103/PhysRevLett.107.035001.
[23] B. Pollock, C. Clayton, J. Ralph, F. Albert, A. Davidson, L. Divol, C. Filip, S. Glenzer, K. Herpoldt, W. Lu, K. Marsh, J. Meinecke, W. Mori, A. Pak, T. Rensink, J. Ross, J. S, Demonstration of a narrow energy spread, ~0.5 GeV electron beam from a two-stage laser wakefield accelerator, Phys. Rev. Lett (2011), http://dx.doi.org/10.1103/PhysRevLett.107.045001.
[24] H.T. Kim, K.H. Pae, H.J. Cha, I.J. Kim, T.J. Yu, J.H. Sung, S.K. Lee, T.M. Jeong, J. Lee, Enhancement of electron energy to the multi-GeV regime by a dual-stage laser-wakefield accelerator pumped by petawatt laser pulses, Phys. Rev. Lett. 111 (2013) 165002, http://dx.doi.org/10.1103/PhysRevLett.111.165002.
[25] W. Wang, W. Li, J. Liu, C. Wang, Q. Chen, Z. Zhang, R. Qi, Y. Leng, X. Liang, Y. Liu, X. Lu, R. Li, Z. Xu, Control of seeding phase for a cascaded laser wakefield accelerator with gradient injection, Appl. Phys. Lett. 103 (2013) 243501, http://dx.doi.org/10.1063/1.4842236.
[26] M. Vargas, W. Schumaker, Z.-H. He, Z. Zhao, K. Behm, V. Chvykov, B. Hou, K. Krushelnick, A. Maksimchuk, V. Yanovsky, A.G.R. Thomas, Improvements to laser wakefield accelerated electron beam stability, divergence, and energy spread using three-dimensional printed two-stage gas cell targets, Appl. Phys. Lett. 104 (2014) 174103, http://dx.doi.org/10.1063/1.4874981.
[27] S. Steinke, J. van Tilborg, C. Benedetti, C.G.R. Geddes, C.B. Schroeder, J. Daniels, K.K. Swanson, A.J. Gonsalves, K. Nakamura, N.H. Matlis, B.H. Shaw, E. Esarey, W.P. Leemans, Multistage coupling of independent laser-plasma accelerators, Nature 530 (2016) 190–193, http://dx.doi.org/10.1038/nature16525.
[28] G. Golovin, S. Chen, N. Powers, C. Liu, S. Banerjee, J. Zhang, M. Zeng, Z. Sheng, D. Umstadter, Tunable monoenergetic electron beams from independently controllable laser-wakefield acceleration and injection, Phys. Rev. Spec. Top. – Accel. Beams 18 (2015) 011301, http://dx.doi.org/10.1103/PhysRevSTAB.18.011301.
[29] M. Zeng, N.A.M. Hafz, K. Nakajima, L.-M. Chen, W. Lu, W.B. Mori, Z.-M. Sheng, J. Zhang, Controlled ionization-induced injection by tailoring the gas-density profile in laser wakefield acceleration, J. Plasma Phys. 78 (2012) 363–371, http://dx.doi.org/10.1017/S0022377812000098.
[30] N.D. Powers, I. Ghebregziabher, G. Golovin, C. Liu, S. Chen, S. Banerjee, J. Zhang, D.P. Umstadter, Quasi-monoenergetic and tunable X-rays from a laser-driven Compton light source, Nat. Photonics. 8 (2013) 28–31, http://dx.doi.org/10.1038/nphoton.2013.314.
[31] C. Liu, S. Banerjee, J. Zhang, S. Chen, K. Brown, J. Mills, N. Powers, B. Zhao, G. Golovin, I. Ghebregziabher, D. Umstadter, Repetitive petawatt-class laser with near-diffraction-limited focal spot and transform-limited pulse duration, in: W.A. Clarkson, R. Shori (Eds.), SPIE LASE, International Society for Optics and Photonics, 2013, pp. 859919–859919–7, http://dx.doi.org/10.1117/12.2005008.
[32] C. Liu, J. Zhang, S. Chen, G. Golovin, S. Banerjee, B. Zhao, N. Powers, I. Ghebregziabher, D. Umstadter, Adaptive-feedback spectral-phase control for interactions with transform-limited ultrashort high-power laser pulses, Opt. Lett. 39 (2013) 80, http://dx.doi.org/10.1364/OL.39.000080.
[33] B. Zhao, J. Zhang, S. Chen, C. Liu, G. Golovin, S. Banerjee, K. Brown, J. Mills, C. Petersen, D. Umstadter, Wavefront-correction for nearly diffraction-limited focusing of dual-color laser beams to high intensities, Opt. Express. 22 (2014) 26947–26955, http://dx.doi.org/10.1364/OE.22.026947.
[34] G. Golovin, S. Banerjee, J. Zhang, S. Chen, C. Liu, B. Zhao, J. Mills, K. Brown, C. Petersen, D. Umstadter, Tomographic imaging of non-symmetric multi-component tailored supersonic flows from structured gas nozzles, Appl. Opt. 54 (2015) 3491–3497, http://dx.doi.org/10.1364/AO.54.003491.
[35] S.P.D. Mangles, G. Genoud, M.S. Bloom, M. Burza, Z. Najmudin, A. Persson, K. Svensson, a G.R. Thomas, C.-G. Wahlström, Self-injection threshold in self-guided laser wakefield accelerators, Phys. Rev. Spec. Top. – Accel. Beams 15 (2012) 011302, http://dx.doi.org/10.1103/PhysRevSTAB.15.011302.
[36] J. Schreiber, C. Bellei, S. Mangles, C. Kamperidis, S. Kneip, S. Nagel, C. Palmer, P. Rajeev, M. Streeter, Z. Najmudin, Complete temporal characterization of asymmetric pulse compression in a laser wakefield, Phys. Rev. Lett. 105 (2010) 1–4, http://dx.doi.org/10.1103/PhysRevLett.105.235003.
[37] M. Chen, E. Esarey, C.B. Schroeder, C.G.R. Geddes, W.P. Leemans, Theory of ionization-induced trapping in laser-plasma accelerators, Phys. Plasmas 19 (2012) 033101, http://dx.doi.org/10.1063/1.3689922.
[38] C. Rechatin, J. Faure, X. Davoine, O. Lundh, J. Lim, A. Ben-Ismaïl, F. Burgy, A. Tafzi, A. Lifschitz, E. Lefebvre, V. Malka, Characterization of the beam loading effects in a laser plasma accelerator, New J. Phys. 12 (2010) 045023, http://dx.doi.org/10.1088/1367-2630/12/4/045023.